Prepublished Copy

NATURE ENVIRONMENT AND POLLUTION TECHNOLOGY

Article In Press

PEER-REVIEWED PREPUBLISHED MANUSCRIPT

This is a peer-reviewed prepublished version of the paper to be published in **Vol. 26, No. 1, March 2027.**

Spatial Distribution and Ecological Risk of Mercury in a Small-Scale Gold-Mining Area of the Upper Ramis Basin, Peru

Fidel Huisa-Mamani, Americo Arizaca-Avalos, Wilber Pastor-Contreras, Mishell Julisa Mamani Flores and Maikol Jordan Huisa Valdivia

RECEIVED
26 April 2026

CITE THIS ARTICLE

Huisa-Mamani, F., Arizaca-Avalos, A., Pastor-Contreras, W., Flores, M.J.M. and Valdivia, M.J.H., 2027. Spatial Distribution and Ecological Risk of Mercury in a Small-Scale Gold-Mining Area of the Upper Ramis Basin, Peru. Nature Environment and Pollution Technology, 26(1), D1938.

https://doi.org/10.46488/NEPT.2027.v26i01.D1938

EARLY-ACCESS STATEMENT

This manuscript, after peer review, is being released online in its original, unedited form to provide early access to its findings. Prior to final publication, it will undergo additional editing and formatting. Readers may note that, as an unedited version, the manuscript may have linguistic and other minor errors. The DOI will be active after the final publication of the paper.

PUBLICATION STATUS

PEER REVIEW	ONLINE VERSION	FINAL ISSUE
Completed	**Prepublished**	**March 2027**

Type of the Paper: Original Research

Spatial Distribution and Ecological Risk of Mercury in a Small-Scale Gold-Mining Area of the Upper Ramis Basin, Peru

Fidel Huisa-Mamani[1] https://orcid.org/0000-0002-6362-9661, Americo Arizaca-Avalos[1] https://orcid.org/0000-0002-0424-0138, Wilber Pastor-Contreras[1] https://orcid.org/0000-0002-5723-0697, Mishell Julisa Mamani Flores[1] https://orcid. org/0009-0003-5082-2272, Maikol Jordan Huisa Valdivia https://orcid.org/0009-0003-9680-6016

[1]Faculty of Mining Engineering, National University of the Altiplano, Puno, Peru Corresponding author: Americo Arizaca-Avalos, aarizaca@unap,edu,pe.
†Corresponding author: A.A.A Dr. aarizaca@unap.edu.pe

Abstract

As both artisanal and small-scale gold mining are significant sources of mercury release in environmentally sensitive Andean headwater systems. This study investigated the spatial distribution and ecological risk of mercury in a high-intensity small-scale gold-mining area in the upper Ramis basin of Peru. The surface water, soil, and vegetation were integrated by means of an analysis. A total of 141 georeferenced samples were collected, including 69 samples from surface water, 47 samples from soil, and 25 samples from vegetation. Total mercury was measured by a DMA-80 direct mercury analyzer. Descriptive statistics, spatial interpolation, heat maps were used to evaluate the dataset, as well as the geoaccumulation index and ecological risk factor, for soil. Mercury appeared to exhibit a good deal of spatial heterogeneity between those three environmental matrices. The surface water concentrations vary from 0.0005 to 0.0942 mg/L and showed a significant hotspot at the final discharge point of the treatment system. The soil contents varied from 0.0046 to 1.3273 mg/kg, with the concentration mainly in ore stockpiling areas, transport corridors and sectors related to camps. Vegetation concentrations were from 0.0051 to 13.8056 mg/kg, which revealed some localized exposure hotspots close to operational infrastructure and vehicle-related areas. Soil risk indices described a limited set of hotspots with high contamination severity and high to very high ecological risk. Finally, the study found that mercury contaminants in this area of study were not diffuse, but were spatially organised according to the operational structure of mining activity. These integrated measures provide a stronger basis for environmental monitoring and territorial prioritization in high-intensity small-scale gold-mining headwater systems.

Keywords

Mercury contamination; small-scale gold mining; upper Ramis basin; geostatistical analysis; ecological risk

1. INTRODUCTION

Artisanal and small-scale gold mining (ASGM) is one of the most widespread extractive activities in low- and middle-income countries. It provides income and employment for millions of people, yet it is also a major source of damage to the environment where extraction and ore processing occur informally, under weak regulatory control and with little environmental management. Recent studies have stressed that ASGM should be recognized as something that does not simply convert resources but is also a socio-environmental process with the potential to transform landscapes, change hydrological pathways, degrade soils, and create long-term exposure risks for ecosystems and nearby populations (Cano & Kunz, 2022; Fritz et al., 2018; Hirons, 2020; Kinyondo & Huggins, 2021; Kohio et al., 2024).

In the mix of all ASGM (e.g., environmental metals), mercury (Hg) is regarded as one of the most serious in its application including applications of all kinds, but remains one of the most critical because it is still widely used in amalgamation processes, persists in environmental media, and poses an enormous environmental and human health hazard. After release, mercury can volatilize into the atmosphere and be redeposited onto soil and water surfaces, bio-accumulated in sediments, and absorbed into food webs. It is a global pollutant with mobility, persistence, and toxicity among the criteria of need for prioritization, particularly in the case of mining areas with scarce environmental monitoring (Crespo-Lopez et al., 2024; Selin & Selin, 2022). Such concerns have also driven global initiatives like the Minamata Convention, which aims to reduce mercury emissions and improve safe alternatives for gold extraction.

Mercury occurrence in mining landscapes is rarely uniform. It is typically multicompartmental and spatially heterogeneous because emission sources, operational areas, hydrological connectivity, atmospheric deposition processes and local disturbance interact across the landscape. Therefore, assessment based on a single environmental matrix may be insufficient to characterize mercury behavior in mining-affected areas. Surface water, soil and vegetation provide complementary evidence: surface water may reflect transport and redistribution pathways, soil may record persistence, deposition and local accumulation, and vegetation, particularly foliar tissue, may indicate environmental exposure through atmospheric deposition or contact with mercury-bearing particles. Accordingly, integrated multicompartment assessments have been increasingly recommended for evaluating contamination processes in mining-affected areas and identifying priority sectors for monitoring and management (McLagan et al., 2025; Setu & Strezov, 2025; Wang et al., 2024).

This issue is particularly relevant in Peru, where artisanal and small-scale gold mining has expanded across Andean and Amazonian territories under conditions of informality or incomplete formalization. This expansion has been associated with environmental concerns such as water contamination, soil degradation, landscape disturbance and weak environmental governance. Recent studies have shown that heavy-metal occurrence related to informal and small-scale mining can be geographically uneven and that geostatistical methods are useful for identifying localized areas of concern. In Mollehuaca, ordinary kriging and exploratory spatial analysis were used to model arsenic and mercury concentrations in mining-affected soils, highlighting the usefulness of spatial methods for interpreting localized contamination patterns and supporting environmental management decisions. Similarly, studies in Madre de Dios have reported that mercury distribution in soil and vegetation in ASGM-affected areas is influenced by local environmental conditions and may reveal relevant pathways of deposition and environmental exposure (Rodriguez-Pascual et al., 2024; Tumy-Gomez et al., 2025).

At the local scale, the upper Ramis basin in southern Peru represents an environmentally sensitive headwater system exposed to sustained pressure from small-scale gold mining. Within this territory, extraction areas, ore-processing sectors, waste-related activities, transport routes, camps, and hydrologically connected downstream environments coexist within a relatively compact but functionally complex mining landscape. In headwater-based mining contexts, mercury pollution is especially relevant because activities in this area may influence environmental quality beyond the immediate operational footprint. However, mercury contamination can affect water, soil, and biota simultaneously, already as detected in previous works in Ananea, where elevated concentrations of mercury can be indicative of active mining and processing sectors in the area (Huisa-Mamani et al., 2025). While the previous work established a crucial baseline, a more spatially explicit understanding is still required to determine how mercury contamination is territorially organized across high-intensity mining sectors, and which operational regions represent the most significant locations of release, redistribution, accumulation, and ecological concern.

This is particularly important since for high-intensity ASGM territories, contamination is affected not only by mercury content, but also by the way in which mining operations structure the landscape. For the latter, discharge points, filtration zones, ore stockpiles, traffic routes, camps, and other operational areas are to some extent potential sources, transport corridors, and retention zones. In this light, we view spatial analysis not just as complementing cartography but as a critical technique for interpreting the organization of contaminant behavior as shaped by mining activity across the territory. Thus, it was postulated that mercury contamination in the study area would not be randomly distributed but rather would exhibit a spatially structured pattern across environmental matrices, with the highest concentrations and ecological risk concentrated in sectors which were functionally related to the operational structure of small-scale gold mining.

In this regard, in the present study it was decided to investigate the spatial distribution and ecological risk of mercury present in a small-scale gold-mining region of the upper Ramis basin, Peru, by incorporating surface water, soil and vegetation-based analysis. In particular, the objectives of the study were: (i) total mercury content in surface water, soil and vegetation; (ii) its spatial distribution and critical hotspots; and (iii) severity of soil contamination based on geoaccumulation index and ecological risk factor. By integrating multiple environmental matrices in a spatial context, this study contributes to a broader understanding of mercury dynamics in a mining-affected headwater system, thus making findings of potentially useful interest to environmental monitoring and management in other high-intensity ASGM areas.

Although the present study is thematically related to the previous work of Huisa-Mamani et al. (2025) in Ananea, the dataset analyzed here is entirely new and independent. None of the 141 sampling points, mercury concentration values, geographic coordinates, or field observations used in the present manuscript were reported or reused in the previous publication. All sampling locations correspond to new georeferenced points collected during September–October 2025 in different operational sectors of the upper Ramis basin. Therefore, the contribution of this study is not a repetition of previous data, but a new spatially explicit multicompartment assessment aimed at identifying mercury hotspots and soil contamination severity in selected mining-affected operational sectors.

2. MATERIALS AND METHODS

2.1 Study area

The study area is the Ramis River basin of the northern portion of the Puno region in southern Peru. This basin is also a component of the endorheic hydrographic system of Lake Titicaca and one of its major tributary regions. It covers the following provinces: Melgar, Azángaro, Carabaya, Sandia, San Antonio de Putina, Lampa, San Román, Moho, and Puno.

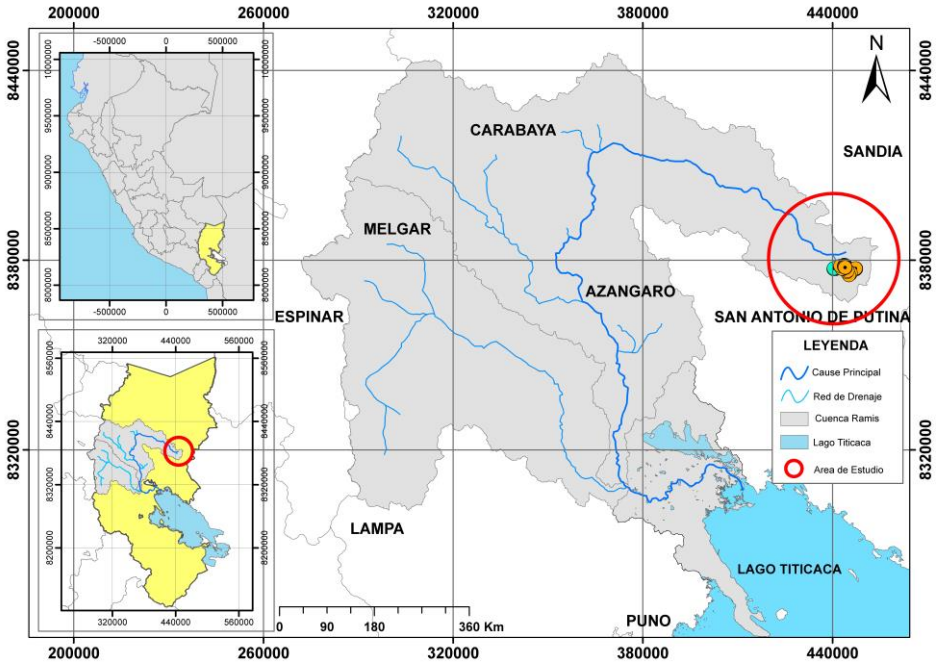

Fig. 1: Geographic location of the Ramis River basin, drainage network, sub-basins, and spatial connection with Lake Titicaca.

As shown in Figure 1, the basin has a well-developed drainage network and several sub-basins linking high Andean headwaters with low reaches in the area near Lake Titicaca. This topographic and sediment hydrology favours the movement of water, sediments, and their possible pollutants from the upstream regions to the lake.

The basin is defined by high Andean relief, significant altitudinal variability, and diverse land use structures including agriculture, livestock cultivation, urban settlements, and extractive operations. At the same time, the Ramis River basin is an environmentally sensitive area because its surface runoff eventually feeds into Lake Titicac.

The sampling area is located in the headwater sector of the Ramis basin, where the Crucero River originates. Downstream, this fluvial system is connected with the Azángaro River and finally contributes to the Ramis River before reaching Lake Titicaca. Therefore, mining activities located in this headwater environment are environmentally relevant not only at the local operational scale but also because they may influence downstream water and sediment pathways within the broader Ramis basin. However, the present study does not claim to represent mercury distribution throughout the entire basin; instead, it focuses on mercury concentrations and operational hotspots within the sampled headwater mining sectors.

2.2 Study design and data sources

This study followed a quantitative, cross-sectional, and non-experimental design based on georeferenced environmental sampling in a high-intensity small-scale gold-mining area of the upper Ramis basin, Peru. The main data source was a field database composed of surface water, soil, and vegetation samples collected in mining-affected sectors.

For each sample, the database included matrix type, geographic coordinates, field observations, and total mercury concentration. Each georeferenced sample was the unit of analysis. The three environmental matrices were chosen because they represent complementary dimensions of mercury transport, accumulation, and exposure in the mining environment. As a result of the multicompartment approach, descriptive, spatial, and ecological risk analyses in the study were based on this multilevel analysis.

The field database used in this study was generated from a new and independent sampling campaign. The 141 georeferenced samples analyzed in the present manuscript, including 69 surface-water samples, 47 soil samples, and 25 vegetation samples, correspond to new sampling points with coordinates different from those reported in previous studies. No analytical values, sampling locations, or field observations from Huisa-Mamani et al. (2025) were reused. This confirms the independence and originality of the dataset used for the present spatial and contamination-severity assessment.

2.3 Environmental sampling

Environmental sampling was conducted during September–October 2025 in selected mining-affected operational sectors of the upper Ramis basin. The sampling design was targeted rather than probabilistic, because the objective was to identify localized mercury hotspots associated with functionally relevant areas of small-scale gold-mining activity. Sampling points were selected in ore-washing areas, drainage pathways, filtration zones, waste-related zones, ore stockpiles, truck traffic routes, vehicle-related areas and mining camps.

A total of 141 georeferenced samples were collected, including 69 surface-water samples, 47 soil samples and 25 vegetation samples. As shown in Fig. 2, the sampling points were distributed across seven operational sectors within the mining-affected headwater area. The spatial coverage of the campaign ranged approximately from 440327.57 to 447381 m E and from 8375260 to 8378489.48 m N in UTM Zone 19S, WGS84 datum. This spatial footprint represents the sampled operational area and should not be interpreted as the full extent of the mining district or the entire upper Ramis basin.

Because the sampling strategy focused on operational sectors where mercury release, transport, accumulation or exposure could occur, the results are suitable for identifying local hotspots and relative spatial patterns within the sampled area. However, they are not intended to provide a statistically representative estimate of mercury distribution across the entire basin. No independent non-mining reference sites were included; therefore, associations between elevated mercury concentrations and mining-related activities were interpreted based on spatial coincidence, field observations and operational context.

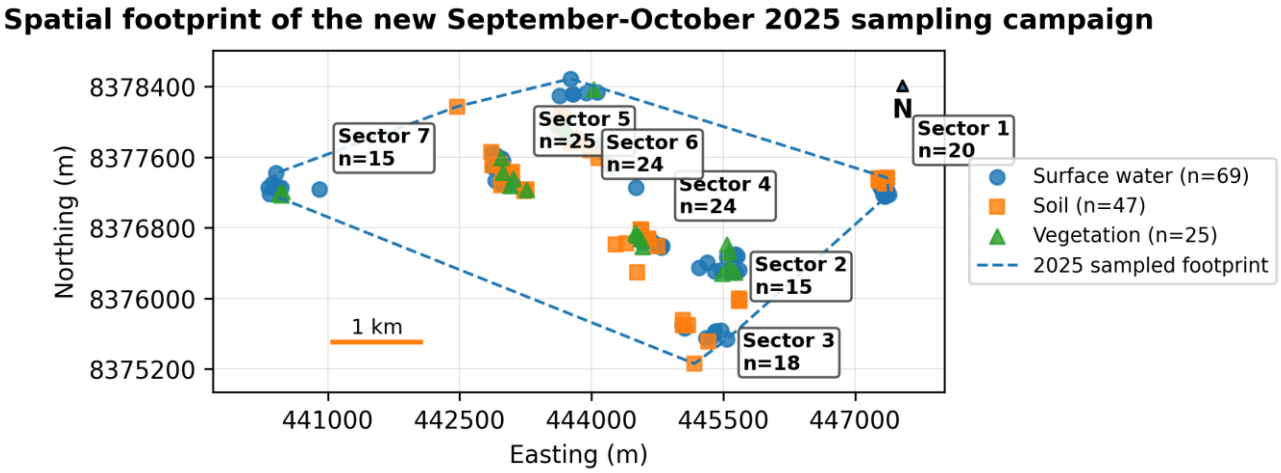

Fig. 2: Spatial footprint of the new September–October 2025 sampling campaign in Ananea, upper Ramis basin, Peru. The map shows 141 georeferenced samples of surface water, soil, and vegetation distributed across seven mining-affected operational sectors. Coordinates are expressed in UTM Zone 19S, WGS84 datum.

2.3.1 Soil sampling

Soil samples were sampled from mining-disturbed zones associated with gold-bearing gravel mining and its related operational activities. Sampling location sampling sites were chosen among sites of high mercury accumulation such as ore stockpiles, areas of tailings, areas of working surfaces and areas of high traffic areas or material handling. Site surface soil samples were taken with clean tools with an emphasis given to the fine upper surface part of the soil layer as mercury gets settled in these surface materials during deposition and continuous exposure. The samples were put into clean, sealed bags and labeled, refrigerated at ~ 4 °C and brought to the lab under chain-of-custody conditions.

2.3.2 Surface water sampling

Samples of surface water from locations influenced by mining activity, such as ore washing sectors, mine drainage connections, filtration zones, and downstream points, were taken. For a representative sample of

the aqueous phase, water was sampled about 20–30 cm below the surface while avoiding disturbance of bottom sediments. The samples were transferred to preconditioned glass bottles, preserved instantly with nitric acid, labeled correctly, refrigerated at approximately 4 °C, and transported to the laboratory under chain-of-custody procedures.

2.3.3 Vegetation sampling

Vegetation sampling focused on foliar tissue from terrestrial plants growing in mining-affected sectors of the study area. The collected vegetation corresponded mainly to two taxonomically identified plant groups: *Onopordum* sp. L. (“cardo”, Asteraceae) and *Stipa* sp. L. (“estipa ichu”, Poaceae), identified by the Plant Taxonomy Laboratory of the National University of the Altiplano, Puno. These taxa were selected because they were present within the sampled operational sectors and could provide evidence of local environmental exposure to mercury.

At each vegetation sampling point, apparently healthy leaves were collected from plants located close to the georeferenced sampling location. The samples were handled with clean stainless-steel tools and gloves, placed in labelled bags, georeferenced, refrigerated at approximately 4 °C and transported to the laboratory for analysis. Leaves were not washed before analysis; therefore, the reported mercury concentrations may include both mercury associated with plant tissue and mercury-bearing particles deposited on leaf surfaces.

2.4 Sample preparation and mercury determination

After collection, all samples were transported to the laboratory under refrigerated conditions and processed according to matrix type. Surface-water samples were homogenized before analysis, and a 0.1 mL aliquot (100 µL) was introduced into clean quartz boats using a micropipette. Soil and vegetation samples were lyophilized for 72 h, homogenized and analyzed as solid matrices. For solid samples, approximately 0.1 g of material was weighed directly into clean quartz boats. Vegetation samples consisted of unwashed foliar tissue; therefore, measured concentrations may include both mercury associated with plant tissue and mercury-bearing particles deposited on leaf surfaces.

Total mercury was determined using a DMA-80 direct mercury analyzer based on thermal decomposition, catalytic conversion, gold amalgamation and atomic absorption spectrophotometry. This technique allows the direct determination of total mercury in liquid and solid environmental samples without acid digestion. The instrumental program included thermal treatment with an increase up to 650 °C, followed by amalgamation and atomic absorption detection. The DMA-80 software recorded the sample code, sample amount, instrumental signal, mercury mass and final concentration, supporting traceability of the analytical sequence. Results were expressed in mg/L for surface water and in mg/kg dry weight for soil and vegetation.

2.5 Quality assurance and quality control

Quality assurance and quality control procedures were applied during field sampling, sample handling and instrumental analysis. In the field, samples were collected using clean materials, labelled immediately, georeferenced and transported to the laboratory under controlled conditions. Before statistical and spatial processing, sample codes, geographic coordinates, matrix type, analytical units and field observations were reviewed to ensure consistency in the database.

Laboratory quality control for total mercury determination included calibration control, analytical blanks and carry-over control during DMA-80 analysis. Calibration was performed using two concentration ranges. The low calibration curve included 0.025, 0.05, 0.10 and 0.15 ppm, whereas the high calibration curve included 0.20, 0.30, 1.0, 2.0, 5.0, 7.0 and 10.0 ppm. The reported method detection limit was 0.01 ppm and the method quantification limit was 0.02 ppm.

To minimize possible cross-contamination and memory effects, analytical blanks were intercalated between sample boats throughout the analytical sequence. The instrumental sequence also included blank readings, calibration or verification standards and burn-out steps of the amalgamator when required. In addition, the DMA-80 auto-blank function was used as an instrumental carry-over control. For samples with high mercury signals, repeated auto-blank readings were performed before continuing with subsequent samples, reducing the risk of mercury carry-over and overestimation in subsequent measurements. The DMA-80 software also provided instrumental statistical summaries for selected analytical groups, including mean concentration, absolute standard deviation and relative standard deviation, which were used as internal checks of signal stability and repeatability.

For solid matrices, soil and vegetation samples were lyophilized for 72 h, homogenized and analyzed using approximately 0.1 g of sample weighed directly into clean quartz boats. Surface-water samples were homogenized and analyzed using a 0.1 mL aliquot (100 µL) introduced into clean quartz boats with a

micropipette. The use of direct mercury analysis avoided acid digestion and reduced potential mercury losses associated with wet-chemistry preparation.

Because certified reference material recovery and duplicate relative percentage difference values were not available in the laboratory report at the time of manuscript revision, these parameters were not reported as formal QA/QC results. Therefore, the analytical quality-control description was based on documented calibration ranges, detection and quantification limits, intercalated analytical blanks, instrumental auto-blank procedures, burn-out steps and software-based signal checks. These controls were used to support analytical traceability and reduce the risk of cross-contamination and carry-over during the DMA-80 analytical sequence.

2.6 Statistical analysis

Subsequently, summary statistics of total mercury concentrations found in surface water, soil, and vegetation were employed. Mean, median, minimum, maximum, standard deviation, coefficient of variation, and skewness were obtained for each environmental matrix to assess central tendency, dispersion, and asymmetry in the data. Before running spatial analysis upon contamination datasets exhibiting heterogeneous distributions and localized extremes, the distribution of mercury concentrations was analyzed. Data cleaning, organization, and statistical processing were performed in Python with pandas.

2.7 Spatial analysis and mapping

Spatial analysis was performed using the georeferenced sampling points recorded in UTM Zone 19S, WGS84 datum. Surface water, soil and vegetation samples were analyzed separately because each matrix represents a different environmental pathway of mercury occurrence, transport, accumulation or exposure. Before interpolation, mercury concentration distributions were examined using descriptive statistics. Because the datasets were strongly right-skewed and influenced by localized high values, mercury concentrations were log10-transformed prior to variogram modelling and ordinary kriging. Extreme values were not removed from the dataset, because they represented field-confirmed hotspot conditions; however, the log10 transformation was used to reduce their disproportionate influence on the interpolation surfaces.

The experimental semivariogram was calculated to evaluate spatial dependence as a function of separation distance, following the classical geostatistical approach proposed by Matheron (1963) and commonly applied in environmental geostatistics (Webster & Oliver, 2007). The semivariance was calculated as.

$$\gamma(h) = \frac{1}{2N(h)} \sum_{i=1}^{N(h)} [Z(x_i) - Z(x_i + h)]^2 \qquad (1)$$

where γ(h) is the semivariance at lag distance h, N(h) is the number of pairs of observations separated by distance h, $Z(x_i)$ is the log10-transformed mercury concentration at location x_i, and $Z(x_i + h)$ is the log10-transformed mercury concentration at a location separated by h. Spherical, exponential and Gaussian models were evaluated, and the final model for each matrix was selected based on visual fit to the experimental semivariogram and leave-one-out cross-validation statistics.

Ordinary kriging was applied as an exploratory interpolation method to visualize relative spatial gradients and potential mercury hotspots within the sampled operational footprint. The ordinary kriging estimator was expressed as:

$$Z^*(x_0) = \sum \lambda i Z(x_i) \qquad (2)$$

where $Z^*(x_0)$ is the estimated log10-transformed mercury concentration at the unsampled location x_0, $Z(x_i)$ is the observed log10-transformed concentration at sampling location x_i, and λ_i represents the kriging weights derived from the fitted semivariogram model. The interpolated values were used only to visualize relative spatial patterns within the sampled operational sectors.

The interpolation grid resolution was set at 50 m. A moving-neighborhood search was applied, using a maximum of 12 neighboring observations for surface water and soil and 8 neighboring observations for vegetation, considering the smaller number of vegetation samples. Directional anisotropy was assessed visually using directional semivariograms; however, anisotropic models were not applied because the targeted and clustered sampling design did not support a stable directional structure. Therefore, isotropic variogram models were used for all matrices.

The main variogram parameters and leave-one-out cross-validation statistics are summarized in Table 1. Cross-validation included mean error (ME), root-mean-square error (RMSE), mean standardized error (MSE) and root-mean-square standardized error (RMSSE). These statistics were used to evaluate the exploratory performance of the interpolation models, not to support basin-wide prediction.

As a complementary visualization tool, heat maps were produced to highlight areas with greater relative concentration intensity in each environmental matrix. These maps do not replace the geostatistical interpolation, but facilitate visual interpretation of hotspot clustering. The resulting spatial outputs were interpreted as exploratory surfaces rather than unrestricted predictive maps. This precaution was especially important for surface water, where Euclidean-distance interpolation does not fully represent hydrological connectivity, and for vegetation, where the sample size was limited to 25 points. Therefore, the spatial outputs were used to support hotspot visualization within the sampled operational sectors, not to infer mercury distribution across the entire upper Ramis basin.

Table 1. Variogram models and leave-one-out cross-validation statistics used for exploratory spatial interpolation.

Matrix	n	Transformation	Selected model	Nugget	Partial sill	Range (m)	Lag interval (m)	Lag classes	Neighbours	ME	RMSE	MSE	RMSSE
Surface water	69	log10(Hg)	Spherical	0.0468	0.0907	518.0	348.4	10	12	-0.008	0.325	-0.024	1.181
Soil	47	log10(Hg)	Exponential	0.2893	0.0266	2834.5	298.4	10	12	-0.011	0.573	-0.019	1.018
Vegetation	25	log10(Hg)	Gaussian	0.4666	0.0434	855.6	504.8	6	8	0.058	0.726	0.078	0.989

2.8 Soil contamination severity and potential ecological risk assessment

Soil contamination severity was assessed using the geoaccumulation index (I_{geo}) the contamination factor (Cf) and the single-metal potential ecological risk factor (Er) for mercury. These indices were applied only to the 47 soil samples, because soil represents a relatively stable matrix for evaluating local mercury accumulation and anthropogenic enrichment in mining-affected areas. The indices were used as screening tools to identify sectors with higher mercury enrichment and potential ecological concern, but they were not interpreted as direct evidence of measured ecological effects or toxicity.

The geoaccumulation index was calculated according to Muller (1969):

$$I_{geo} = \log_2\left(\frac{C_n}{1.5B_n}\right) \quad (3)$$

where C_n is the measured mercury concentration in each soil sample and B_n is the geochemical background concentration. The factor 1.5 was included to account for possible natural lithological variability. In this study, the background value adopted for mercury in soil was 0.056 mg/kg for mercury. This value was adopted as a literature-based geochemical reference corresponding to the mercury abundance reported for the upper continental crust by Wedepohl (1995). Because no independent non-mining local background soils were collected during the present campaign, this value was not interpreted as a measured local background for the upper Ramis basin. Therefore, Igeo results should be interpreted as a comparative contamination-severity screening based on a literature reference value.

The Igeo values were classified as follows: uncontaminated (Igeo ≤ 0), uncontaminated to moderately contaminated (0 < Igeo ≤ 1), moderately contaminated (1 < Igeo ≤ 2), moderately to strongly contaminated (2 < Igeo ≤ 3), strongly contaminated (3 < Igeo ≤ 4), strongly to extremely contaminated (4 < Igeo ≤ 5) and extremely contaminated (Igeo > 5).

The contamination factor was calculated as:

$$Cf = Cn/Bn \quad (4)$$

where Cf is the contamination factor, Cn is the measured mercury concentration in soil and Bn is the adopted geochemical reference value. The single-metal potential ecological risk factor was calculated following Hakanson (1980):

$$Er = Tr \times Cf \quad (5)$$

where Er is the single-metal potential ecological risk factor, Tr is the toxic-response factor and Cf is the contamination factor. For mercury, Tr was set at 40, following the conventional application of the Håkanson approach for trace-metal risk assessment. The Er values were classified as low risk (Er < 40), moderate

risk (40 ≤ Er < 80), considerable risk (80 ≤ Er < 160), high risk (160 ≤ Er < 320) and very high risk (Er ≥ 320).

Although the Håkanson approach was originally developed for sediment contamination assessment, it has also been applied as a comparative screening tool in soil studies affected by mining and other anthropogenic activities. In the present study, Er was interpreted only as a single-metal potential ecological risk factor for mercury in soil, not as a comprehensive multi-element ecological risk index. Consequently, the terms “potential ecological risk” and “contamination severity” refer to index-based screening results within the sampled operational sectors and do not imply measured ecological toxicity
.

2.9 Interpretation framework

The analytical and spatial results were interpreted using an integrated multicompartment framework. Surface-water results were interpreted as evidence of mercury occurrence and redistribution in hydraulically connected sectors, including discharge points, filtration zones, water-capture structures, and downstream sampling points. Soil results were interpreted in relation to mercury accumulation, anthropogenic enrichment, and potential ecological concern using concentration values, spatial patterns, *(Igeo),* and *(Er).* Vegetation results were interpreted as evidence of environmental exposure in areas functionally linked to mining operations, particularly operational infrastructure and vehicle-related sectors.

Because the sampling design was targeted and focused on selected mining-affected operational sectors, the interpretation was restricted to the sampled operational footprint. The spatial outputs were used to identify relative gradients and potential hotspots, but not to infer mercury distribution across the entire upper Ramis basin. Likewise, associations between elevated mercury concentrations and mining-related activities were interpreted based on spatial coincidence, field observations, and operational context, rather than as direct causal evidence. Since sampling was conducted only during September–October 2025, the results represent the conditions observed during that field campaign and do not describe seasonal or year-round variability.

Surface-water mercury concentrations were compared with the Peruvian Environmental Quality Standards for Water approved by Supreme Decree No. 004-2017-MINAM. Considering the high-Andean river setting of the study area and its hydrological connection with the Titicaca basin, the comparison was made using Category 4, Subcategory E2: Rivers – Coast and Highlands, for which the environmental quality standard for total mercury is 0.0001 mg/L. This comparison was used as a regulatory screening reference for surface-water quality. However, because several sampling points corresponded to operational ponds, filtration zones, water-capture structures or discharge-related points, the comparison should not be interpreted as a formal compliance assessment for all samples. In particular, for treated-water discharges, ECA compliance should be evaluated in the receiving natural water body outside the mixing zone, according to the regulatory framework

3. RESULTS

Mercury concentrations showed pronounced spatial heterogeneity among the three environmental matrices within the sampled operational footprint. The highest values were concentrated in specific operational sectors and reflected different patterns of occurrence, accumulation or environmental exposure depending on the matrix analyzed. Surface water mainly reflected mercury occurrence in hydraulically connected sectors, soil showed localized accumulation in disturbed operational surfaces, and vegetation indicated environmental exposure in foliar tissue near infrastructure and vehicle-related areas.

3.1 Mercury concentrations in surface water

Mercury concentrations showed pronounced variability among the three environmental matrices within the sampled operational footprint. The highest values were concentrated in specific sectors associated with discharge points, filtration zones, ore stockpiling areas, transport corridors, vehicle-related areas, and mining camps. These patterns are presented as descriptive and exploratory results for the September–October 2025 sampling campaign and should be interpreted within the sampled operational sectors rather than as a basin-wide estimate of mercury contamination.

Table 2: Surface water sampling points with the highest total mercury concentrations and their location within the study area.

Code	Concentration	Unit	Field observations	Easting	Northing
MA-38	0.0942	mg/L	Sample collected at the final discharge point of the treatment system	444795.000	8376576.000

MA-34	0.0162	mg/L	Water capture pond No. 02	444571.000	8376639.000
MA-52	0.0061	mg/L	Filtration area	443936.669	8378326.434
MA-03	0.0049	mg/L	Outlet of P.S.	447362.000	8377221.000
MA-22	0.0040	mg/L	Not determined	445038.000	8375693.000

Table 2 shows the surface-water sampling points with the highest total mercury concentrations. The maximum value was recorded at point MA-38 (0.0942 mg/L), located at the final discharge point of the treatment system. This was followed by MA-34 (0.0162 mg/L), associated with water capture pond No. 02; MA-52 (0.0061 mg/L), located in a filtration area; MA-03 (0.0049 mg/L), corresponding to an outlet point; and MA-22 (0.0040 mg/L). Spatially, the highest mercury concentrations were located in sectors associated with discharge, water capture, filtration, and outlet zones. Point MA-38 represented the main surface-water hotspot, while lower secondary hotspots were observed in other hydraulically connected operational sectors (Figure 3). The heat map also showed a clustering of elevated values around the main hydraulic nodes of the sampled mining system (Figure 4), indicating a pronounced but spatially localized distribution of mercury in surface water within the sampled operational footprint.

To provide a regulatory screening context, surface-water mercury concentrations were compared with the Peruvian Environmental Quality Standard for Water, Category 4, Subcategory E2: Rivers – Coast and Highlands, which establishes a mercury reference value of 0.0001 mg/L for total mercury. As shown in Table 3, all 69 surface-water samples exceeded this reference value. The maximum concentration recorded at MA-38 (0.0942 mg/L), located at the final discharge point of the treatment system, exceeded the ECA reference value by approximately 942 times. This result identifies MA-38 as the principal discharge-related hotspot within the sampled operational footprint. However, because several sampling points corresponded to operational ponds, filtration zones, water-capture structures or discharge-related locations, this comparison should be interpreted as a regulatory screening reference rather than as a formal compliance assessment for the entire receiving water body.

Table 3. Regulatory screening of surface-water mercury concentrations against the Peruvian Environmental Quality Standard for Water.

Reference criterion	Hg limit (mg/L)	Surface-water simples (n)	Samples exceeding the limit	Samples exceeding the limit (%)	Maximum value (mg/L)	Maximum exceedance
ECA Water, Category 4, E2 Rivers – Coast and Highlands	0.0001	69	69	100%	0.0942	942 times

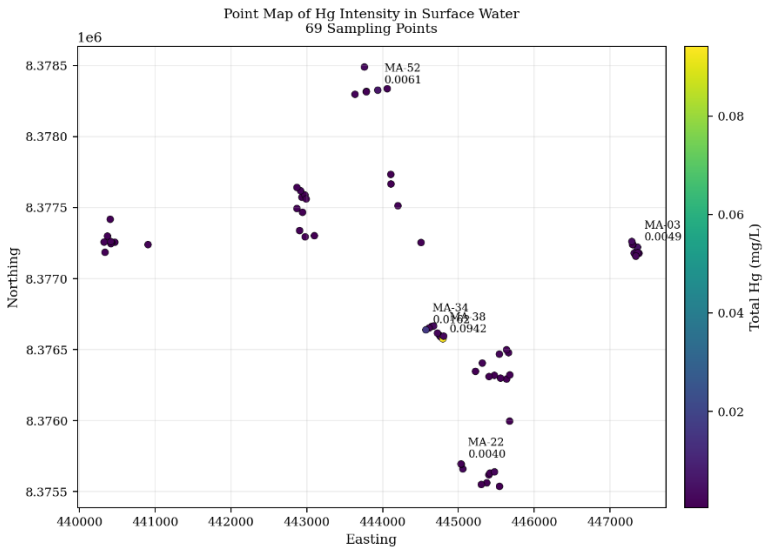

Fig. 3: Spatial distribution of total mercury concentrations in surface water in the study area.

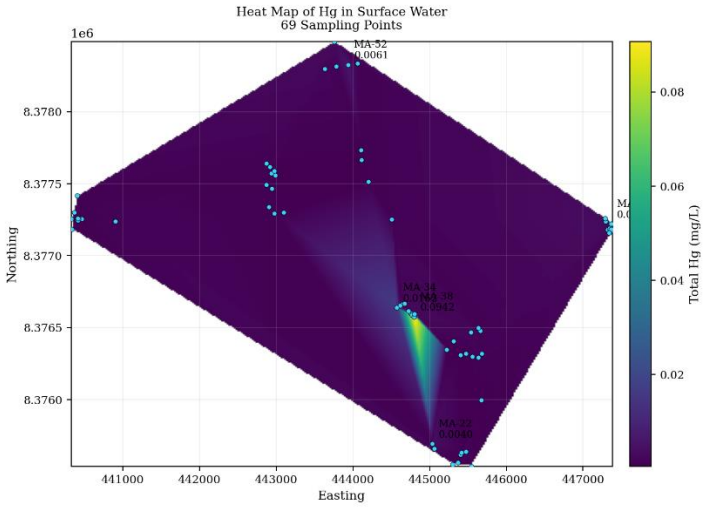

Fig. 4: Heat map of total mercury concentrations in surface water in the study area.

3.2 Mercury concentrations in soil

Mercury concentrations in soil showed pronounced spatial variability within the sampled operational footprint. A total of 47 soil samples were analyzed, with a mean concentration of 0.1025 mg/kg and a median of 0.0351 mg/kg. Concentrations ranged from 0.0046 to 1.3273 mg/kg, with a standard deviation of 0.2169 mg/kg, a coefficient of variation of 211.68%, and a skewness of 4.4407. These values indicate an asymmetric distribution influenced by a limited number of samples with elevated mercury concentrations.

Table 4: Soil sampling points with the highest total mercury concentrations and their location within the sampled operational footprint.

Code	Concentration	Unit	Field observations	Easting	Northing
MS-03	1.3273	mg/kg	Mineral storage area	447363.000	8377366.000
MS-37	0.5755	mg/kg	This sample was collected along the edge of sector No. 1	444276.000	8376610.000
MS-04	0.4301	mg/kg	Fine ore storage area	447358.000	8377364.000
MS-59	0.4164	mg/kg	The sample was taken from the upper section where the trucks were driving. From Mosog Mine	444080.574	8377590.872
MS-45	0.2189	mg/kg	The sample was obtained inside the mining camp, near the vehicle parking area..	443004.081	8377371.187

Table 4 presents the soil sampling points with the highest total mercury concentrations. The maximum value was recorded at point MS-03 (1.3273 mg/kg), located in a mineral storage area. This was followed by MS-37 (0.5755 mg/kg), collected along the edge of sector No. 1; MS-04 (0.4301 mg/kg), located in a fine ore storage area; MS-59 (0.4164 mg/kg), associated with the upper section of a truck circulation route in Mosog Mina; and MS-45 (0.2189 mg/kg), collected inside the mining camp near a vehicle parking area.

Spatially, the highest soil mercury concentrations were located in ore storage areas, transport corridors, and camp-related spaces. The exploratory interpolation surface showed localized hotspots within these operationally disturbed sectors rather than a uniform distribution across the sampled area (Figure 5). Similarly, the heat map highlighted relative concentration intensity around areas associated with ore handling, vehicle movement, and camp infrastructure (Figure 6). These results suggest that mercury enrichment in soil was spatially localized within specific operational sectors of the sampled mining area.

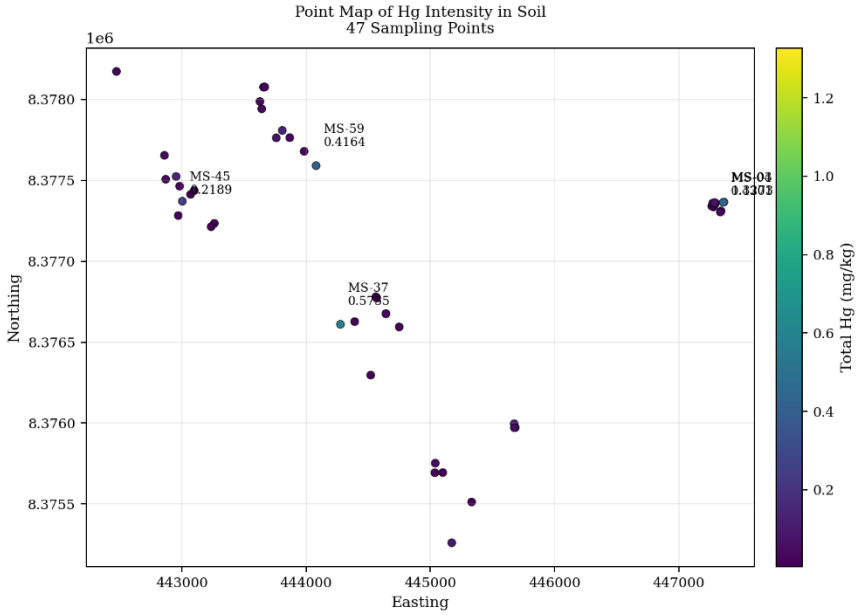

Fig. 5: Spatial distribution of total mercury concentrations in soil in the study area.

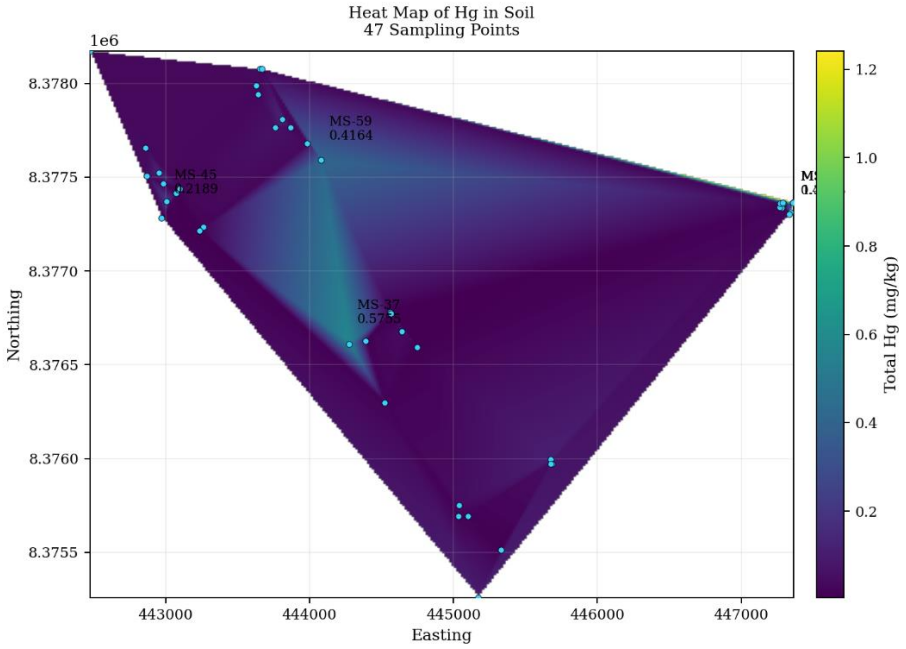

Fig. 6: Heat map of total mercury concentrations in soil in the study area.

3.3 Mercury concentrations in vegetation

Mercury concentrations in vegetation showed pronounced variability within the sampled operational footprint. A total of 25 vegetation samples were analyzed, with a mean concentration of 0.8089 mg/kg and a median of 0.1101 mg/kg. Concentrations ranged from 0.0051 to 13.8056 mg/kg, with a standard deviation of 2.7391 mg/kg, a coefficient of variation of 338.62%, and a skewness of 4.8228. These descriptive statistics indicate a highly asymmetric distribution influenced by a small number of samples with elevated mercury concentration.

Table 5. Vegetation sampling points with the highest total mercury concentrations and their location within the study area.

Code	Concentration	Unit	Field observations	Easting	Northing
MB-34	13.8056	mg/kg	This sample was taken next to the vehicle station.	444557.870	8376674.990

MB-55	1.5665	mg/kg	The flora was removed from where the lightning rod is located.	443714.921	8377847.586
MB-14	1.2262	mg/kg		445562.840	8376366.974
MB-35	1.1584	mg/kg	This sample was taken 5 meters from the S.S.H	444575.000	8376583.000
MB-13	0.3942	mg/kg	Not determined	445634.118	8376293.003

Table 5 presents the vegetation sampling points with the highest mercury concentrations. The maximum value was recorded at point MB-34 (13.8056 mg/kg), collected next to the vehicle station. This was followed by MB-55 (1.5665 mg/kg), collected near the lightning rod area; MB-14 (1.2262 mg/kg); MB-35 (1.1584 mg/kg), collected approximately 5 m from the sanitary services area; and MB-13 (0.3942 mg/kg). These values indicate that the highest vegetation-associated mercury concentrations were localized in areas close to operational infrastructure and vehicle-related activity.

The exploratory interpolation surface showed a localized hotspot around MB-34, while the remaining elevated values appeared as smaller and spatially restricted concentration signals (Figure 7). The heat map similarly showed relative concentration intensity in specific operational sectors rather than a uniform pattern across the sampled area (Figure 8). Because vegetation samples may reflect both external deposition of mercury-bearing particles on leaf surfaces and plant-associated accumulation, these results are interpreted as evidence of environmental exposure in vegetation within the sampled operational footprint, rather than as direct evidence of internal biological uptake.

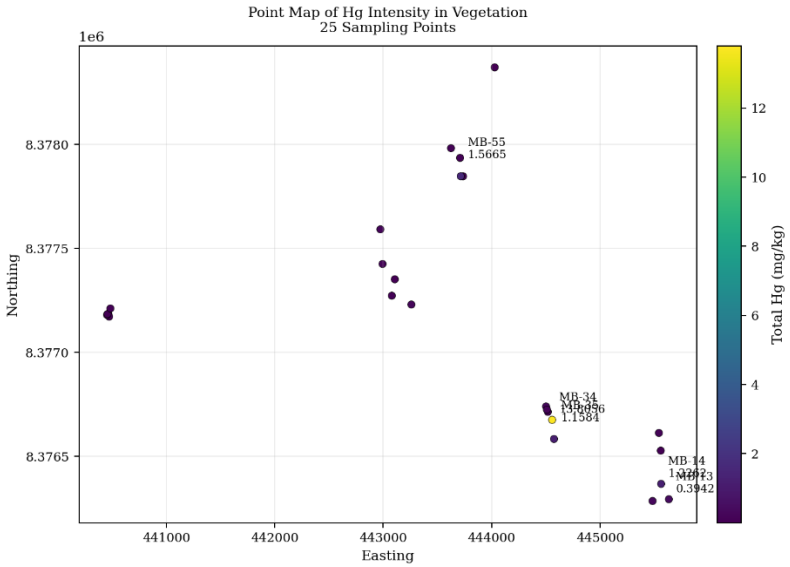

Fig. 7: Spatial distribution of total mercury concentrations in vegetation in the study area.

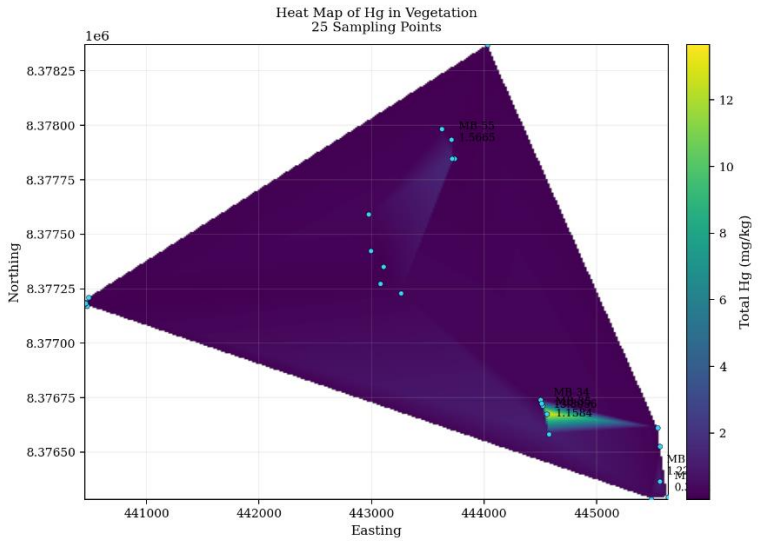

Fig. 8: Heat map of total mercury concentrations in vegetation in the study area.

The exploratory interpolation surface showed a localized hotspot around MB-34, while the remaining elevated values appeared as smaller and spatially restricted concentration signals (Figure 7). The heat map similarly showed relative concentration intensity in specific operational sectors rather than a uniform pattern across the sampled area (Figure 8). Because vegetation samples corresponded to unwashed foliar tissue of *Onopordum* sp. L. and *Stipa* sp. L., the results should be interpreted considering possible differences in plant characteristics and exposure conditions. The highest value recorded at MB-34, located next to a vehicle station, should be interpreted with particular caution because mercury-bearing dust or particles deposited on leaf surfaces may have contributed to the measured concentration. Therefore, vegetation results are interpreted as evidence of environmental exposure in foliar tissue within the sampled operational footprint, rather than as direct evidence of internal biological uptake or species-specific bioaccumulation.

3.4 Comparative spatial pattern across matrices

The comparison of the three environmental matrices showed matrix-specific spatial patterns within the sampled operational footprint. In surface water, the highest mercury concentrations were associated with hydraulically connected sectors, including discharge, water-capture, filtration, and outlet points. In soil, the highest concentrations were mainly located in ore storage areas, transport corridors, and camp-related spaces. In vegetation, elevated mercury concentrations were observed near operational infrastructure and vehicle-related sectors.

Overall, the spatial pattern suggests that mercury occurrence was not uniformly distributed across the sampled area. Instead, each environmental matrix reflected a different component of the contamination process: surface water represented possible transport and redistribution pathways, soil reflected localized accumulation in disturbed operational surfaces, and vegetation indicated environmental exposure in areas close to mining-related infrastructure. These results should be interpreted as exploratory evidence of localized mercury hotspots within the sampled operational sectors, rather than as a general spatial pattern for the entire upper Ramis basin.

3.5 Geoaccumulation index and ecological risk in soil

The geoaccumulation index (Igeo), contamination factor (Cf) and single-metal potential ecological risk factor (Er) were calculated for the 47 soil samples using the adopted literature-based geochemical reference value of 0.056 mg/kg. Because this value does not represent a locally measured background for the upper Ramis basin, the resulting classifications should be interpreted as comparative screening indicators of soil contamination severity and potential ecological concern within the sampled operational sectors.

The (Er) values ranged from 3.29 to 948.07, with a mean of 73.18 and a median of 25.07. According to the single-metal potential ecological risk classification, 33 samples showed low risk, 5 moderate risk, 5 considerable risk, 2 high risk, and 2 very high risk. These results indicate that most soil samples showed low mercury enrichment and low potential ecological concern, while a limited number of samples concentrated the highest contamination-severity and risk-index values.

The soil points with the highest contamination severity are shown in Table 6. Point MS-03, located in an ore stockpiling area, recorded the highest mercury concentration (1.3273 mg/kg), with an (Igeo) value of 3.9820 and an (Er) value of 948.07. This point was classified as strongly contaminated and showed very high single-metal potential ecological risk. Point MS-37 (0.5755 mg/kg) showed an (Igeo) value of 2.7784 and an (Er) value of 411.07, corresponding to moderately to strongly contaminated soil and very high potential ecological risk. Points MS-04 and MS-59 were classified as moderately to strongly contaminated and showed high potential ecological risk, whereas MS-45 was classified as moderately contaminated with considerable potential ecological risk.

Overall, the index-based results indicate that soil contamination severity was not uniformly distributed within the sampled operational footprint. Instead, the highest (Igeo) and (Er) values were concentrated in a small number of operationally disturbed sectors, particularly ore storage areas, transport routes, and camp-related spaces. These results should be interpreted as screening-level indicators of mercury enrichment and potential ecological concern in soil, not as direct evidence of measured ecological effects.

Table 6. Soil sampling points with the highest mercury contamination severity and single-metal potential ecological risk.

Code	Hg (mg/kg)	Igeo	Igeo category	Er (= RI)	Risk category	Field observation

MS-03	1.3273	3.982	Strongly contaminated	948.07	Very high	Ore stockpiling area
MS-37	0.5755	2.7784	Moderately to strongly contaminated	411.07	Very high	This sample was collected along the edge of sector No. 1
MS-04	0.4301	2.3571	Moderately to strongly contaminated	307.21	High	Fine ore stockpiling area
MS-59	0.4164	2.3104	Moderately to strongly contaminated	297.43	High	Upper section of the truck circulation route in Mosog Mina
MS-45	0.2189	1.3823	Moderately contaminated	156.36	Considerable	Inside the mining camp, near the vehicle parking area

4. DISCUSSION

4.1 Multicompartment behavior of mercury in the sampled mining sectors

The results show that mercury occurrence in the sampled mining sectors cannot be adequately interpreted from a single environmental matrix. Surface water, soil, and vegetation reflected complementary components of the same contamination context. Surface water showed the most evident mercury signal in hydraulically connected points, particularly discharge, filtration, water-capture, and outlet sectors. Soil reflected localized accumulation in operationally disturbed surfaces, especially ore storage areas, transport corridors, and camp-related spaces. Vegetation showed elevated mercury concentrations in areas close to operational infrastructure and vehicle-related sectors.

This multicompartment pattern is consistent with the behavior of mercury in artisanal and small-scale gold-mining environments, where releases may be redistributed through water pathways, deposited on exposed surfaces, retained in soils, or associated with plant surfaces and tissues. Mercury does not necessarily remain at the point of release; instead, its distribution may depend on emission intensity, hydrological connectivity, surface disturbance, atmospheric deposition, particle transport, and local retention processes (Crespo-Lopez et al., 2024; Selin & Selin, 2022; Wang et al., 2024).

However, the interpretation of each matrix must be differentiated. Surface water should be understood mainly as evidence of active or recent redistribution within connected hydraulic sectors. Soil provides evidence of localized enrichment and persistence in disturbed operational areas. Vegetation should be interpreted as an environmental exposure signal rather than direct evidence of internal biological uptake, because mercury measured in leaves may reflect both atmospheric deposition or mercury-bearing particles on plant surfaces and plant-associated accumulation. This distinction is important, especially for samples collected near vehicle-related areas, where dust resuspension and external deposition may contribute to elevated values.

The present results complement previous work in Ananea by providing a new and independent spatially explicit dataset for selected operational sectors. While previous studies established the relevance of mercury contamination in water, soil, and biota in the district, the present study shows how mercury concentrations are organized within a new sampled operational footprint, where different matrices reveal different expressions of contamination. Therefore, the main contribution is not a basin-wide estimate, but an integrated characterization of localized hotspots and contamination-severity patterns in selected mining-affected sectors.

4.2 Spatial controls and soil contamination severity

The spatial pattern observed in this study suggests that mercury concentrations were not uniformly distributed within the sampled operational footprint. Higher values were located in sectors functionally related to discharge points, water-capture structures, filtration areas, ore stockpiles, transport routes, vehicle-related spaces, and camps. These findings indicate a close spatial association between elevated mercury concentrations and the operational structure of small-scale gold mining. Nevertheless, because the sampling design was targeted and no independent non-mining reference sites were included, these associations should be interpreted as spatial and operational evidence rather than as direct causal proof.

In surface water, the main hotspot was located at the final discharge point of the treatment system, while secondary elevated values were observed in other hydraulically connected locations. This pattern suggests that hydraulic nodes may play an important role in mercury redistribution within the sampled mining system. However, the spatial interpolation for surface water should be interpreted cautiously because Euclidean-distance interpolation does not fully represent flow direction, drainage connectivity, or transport along the hydrological network.

In soil, the highest mercury concentrations and the highest index-based contamination severity values were concentrated in ore stockpiling areas, truck circulation routes, and camp-related spaces. This pattern is consistent with the role of disturbed operational surfaces as potential accumulation zones for mercury-bearing particles. Similar spatial associations have been reported in mining-affected environments, where transport, storage, processing, and repeatedly disturbed surfaces can concentrate metal contamination (Ndzana et al., 2023; Setu & Strezov, 2025; Tumy-Gomez et al., 2025).

The geoaccumulation index and the single-metal potential ecological risk factor provided additional evidence of localized soil contamination severity. Most soil samples showed low enrichment or low potential ecological concern, but a small number of samples concentrated the highest (Igeo) and (Er) values. This indicates that average concentrations alone may underestimate the importance of localized hotspots. However, (Er) should be interpreted only as a screening-level single-metal potential ecological risk factor for mercury in soil, not as evidence of measured ecological effects or as a comprehensive multi-element ecological risk index.

4.3 Implications for monitoring and territorial prioritization

The findings have practical implications for environmental monitoring in high-intensity small-scale gold-mining areas. First, the results suggest that monitoring should not focus only on ore-processing or discharge points. Other operationally connected sectors, such as filtration areas, ore stockpiles, transport routes, vehicle-related spaces, and camps, may also require attention because they can act as zones of accumulation, redistribution, or exposure.

Second, the three environmental matrices provide different but complementary information. Surface water is useful for identifying possible transport and redistribution pathways. Soil is useful for detecting persistent enrichment and contamination-severity hotspots. Vegetation can provide an additional environmental exposure signal in areas affected by infrastructure, traffic, dust, and atmospheric deposition. Therefore, an integrated monitoring strategy should combine water, soil, and vegetation rather than relying on a single matrix.

Third, the spatial concentration of hotspots suggests that territorial prioritization may be more efficient than uniform monitoring across the entire mining area. In contexts with limited technical and institutional resources, priority should be given to sectors where elevated mercury concentrations, operational disturbance, and potential exposure pathways overlap. This approach may support more focused sampling, remediation planning, control of dust-generating activities, improved management of stockpiles, and periodic evaluation of discharge and filtration zones.

4.4 Limitations and scope of interpretation

Several limitations should be considered when interpreting the results. The sampling design was targeted toward mining-affected operational sectors and was not intended to represent the entire upper Ramis basin. Therefore, the results identify localized mercury hotspots and contamination-severity patterns within the sampled operational footprint, but they should not be generalized as basin-wide mercury distribution.

The study was also cross-sectional, with sampling conducted during September–October 2025. Seasonal changes in rainfall, runoff, streamflow, mining intensity, dust deposition, and vegetation condition were not evaluated. As a result, the findings describe the conditions observed during the sampling campaign and do not demonstrate year-round persistence of the same spatial patterns.

The spatial interpolation maps should also be interpreted as exploratory surfaces. Although log-transformed data, variogram fitting, and leave-one-out cross-validation were used, the sampling distribution was clustered by operational sectors. In addition, the vegetation dataset contained only 25 samples, which limits the robustness of variogram estimation. For surface water, hydrological connectivity may be more relevant than Euclidean distance. Therefore, the maps are useful for visualizing relative gradients and potential hotspots, but not for making unrestricted spatial predictions.

Finally, vegetation results should be interpreted with caution because species-level differences, washing procedures, and the distinction between external particle deposition and internal uptake can influence mercury concentrations. Future studies should include standardized vegetation preparation, species identification, non-mining reference sites, seasonal sampling, hydrological-network-based spatial analysis for water, and a broader suite of metals to strengthen ecological-risk interpretation.

5. CONCLUSIONS

This study evaluated mercury concentrations in surface water, soil, and vegetation within selected mining-affected operational sectors of the upper Ramis basin during the September–October 2025 sampling campaign. The results showed a pronounced multicompartment pattern within the sampled operational footprint. Surface water reflected mercury occurrence in hydraulically connected sectors, soil showed localized accumulation in operationally disturbed areas, and vegetation indicated environmental exposure in areas close to infrastructure and vehicle-related activity.

The highest mercury concentrations were not evenly distributed across the sampled area, but were concentrated in specific sectors such as discharge points, filtration zones, ore stockpiling areas, transport routes, vehicle-related areas, and mining camps. These findings suggest that mercury occurrence in the sampled mining sectors was spatially localized and operationally structured. However, because the sampling design was targeted and no independent non-mining reference sites were included, these associations should be interpreted as spatial and operational evidence rather than direct causal proof.

In soil, the geoaccumulation index and the single-metal potential ecological risk factor identified a limited number of hotspots with higher mercury enrichment and greater potential ecological concern. Most soil samples showed low contamination severity and low potential ecological risk, whereas the highest index values were concentrated in a small number of operationally disturbed sectors. These index-based results should be interpreted as screening-level indicators of mercury contamination severity, not as direct evidence of measured ecological effects or toxicity.

Overall, the study provides a new and independent spatially explicit dataset for mercury assessment in selected operational sectors of Ananea. The findings support the use of integrated monitoring strategies combining surface water, soil, and vegetation to identify localized hotspots and prioritize environmental management. Nevertheless, the results are restricted to the sampled operational footprint and to the September–October 2025 field campaign; therefore, they should not be generalized to the entire upper Ramis basin or interpreted as year-round contamination patterns without additional seasonal and reference-site monitoring.

6. ACKNOWLEDGMENTS

The authors gratefully acknowledge the financial support provided by the National University of the Altiplano, through its Vice-Rectorate for Research, for the development of this study. The authors also acknowledge the technical and logistical support provided by the Faculty of Mining Engineering of the National University of the Altiplano, Puno, Peru, during field sampling, sample handling, and laboratory coordination. This research was funded by the National University of the Altiplano, through its Vice-Rectorate for Research.

7. REFERENCES

Cano, Á., & Kunz, N. C. (2022). Large-scale and small-scale mining in Peru: Exploring the interface. *Resources Policy*, *76*, 102530. https://doi.org/https://doi.org/10.1016/j.resourpol.2021.102530

Crespo-Lopez, M. E., Lopes-Araújo, A., Basta, P. C., Soares-Silva, I., de Souza, C. B. A., Leal-Nazaré, C. G., Santos-Sacramento, L., Barthelemy, J. L., Arrifano, G. P., & Augusto-Oliveira, M. (2024). Environmental pollution challenges public health surveillance: the case of mercury exposure and intoxication in Brazil. *The Lancet Regional Health - Americas*, *39*, 100880. https://doi.org/https://doi.org/10.1016/j.lana.2024.100880

Fritz, M. M., McQuilken, J., Collins, N., & Weldegiorgis, F. (2018). Global Trends in Artisanal and Small-Scale Mining (ASM): A review of key numbers and issues. *HAL Working Papers*(hal-02547257).

Hakanson, L. (1980). An ecological risk index for aquatic pollution control. A sedimentological approach. *Water Research*, *14*(8), 975-1001.

Hirons, M. (2020). How the Sustainable Development Goals risk undermining efforts to address environmental and social issues in the small-scale mining sector. *Environmental Science & Policy*, *114*, 321-328. https://doi.org/https://doi.org/10.1016/j.envsci.2020.08.022

Huisa-Mamani, F., Arizaca-Avalos, A., & Llanque-Maquera, O. E. (2025). Mercury pollution in water, soil, and biota induced by artisanal gold mining: A case study from Ananea District, Puno, Peru. *Journal of Degraded and Mining Lands Management*, *12*(2), 7159-7171. https://doi.org/10.15243/jdmlm.2025.122.7159

Kinyondo, A., & Huggins, C. (2021). State-led efforts to reduce environmental impacts of artisanal and small-scale mining in Tanzania: Implications for fulfilment of the sustainable development goals. *Environmental Science & Policy*, *120*, 157-164. https://doi.org/https://doi.org/10.1016/j.envsci.2021.02.017

Kohio, E. N. B., Karoui, H., Sossou, S. K., & Yacouba, H. (2024). Review of pollution trends and impacts in artisanal and small-scale gold mining in Sub-Saharan Africa: Advancing towards sustainable practices through equitable redistribution of gold spin-offs. *Journal of Cleaner Production*, *476*, 143754. https://doi.org/https://doi.org/10.1016/j.jclepro.2024.143754

Matheron, G. (1963). " Principles of geostatistics", Economic Geology, 58, pp 1246-1266.

McLagan, D. S., Eboigbe, E. O., & Strickman, R. J. (2025). Reviews and syntheses: Artisanal and small-scale gold mining (ASGM)-derived mercury contamination in agricultural systems: what we know and need to know. *Biogeosciences*, *22*(21), 6695-6726. https://doi.org/10.5194/bg-22-6695-2025

Muller, G. (1969). Index of geoaccumulation in sediments of the Rhine River.

Rodriguez-Pascual, M. J., Vega, C. M., Andrade, N., Fernández, L. E., Silman, M. R., & Torrents, A. (2024). “Hg distribution and accumulation in soil and vegetation in areas impacted by artisanal gold mining in the Southern Amazonian region of Madre de Dios, Peru.”. *Chemosphere*, *361*, 142425. https://doi.org/https://doi.org/10.1016/j.chemosphere.2024.142425

Selin, H., & Selin, N. E. (2022). From Stockholm to Minamata and beyond: Governing mercury pollution for a more sustainable future. *One Earth*, *5*(10), 1109-1125. https://doi.org/https://doi.org/10.1016/j.oneear.2022.09.001

Setu, S., & Strezov, V. (2025). Impacts of non-ferrous metal mining on soil heavy metal pollution and risk assessment. *Science of The Total Environment*, *969*, 178962. https://doi.org/https://doi.org/10.1016/j.scitotenv.2025.178962

Tumy-Gomez, E. H., Arizaca-Avalos, A., Huisa-Mamani, F., Apaza-Chino, J., & Pastor-Contreras, W. (2025). Geostatistical modeling of soil contamination by arsenic and mercury in Mollehuaca, Peru. *Journal of Degraded and Mining Lands Management*, *12*(5), 8547-8559. https://doi.org/10.15243/jdmlm.2025.125.8547

Wang, D., Li, Z., & Wang, Q. (2024). Ecological restoration reduces mercury in corn kernel and the distinction of mercury in corn plants in rural China – A case in Wuchuan mercury mining area. *Ecotoxicology and Environmental Safety*, *271*, 115964. https://doi.org/https://doi.org/10.1016/j.ecoenv.2024.115964

Webster, R., & Oliver, M. A. (2007). *Geostatistics for environmental scientists*. John Wiley & Sons.

8. BACKGROUND INFORMATION FOR RECORD (NOT TO BE PRINTED)

Author Contributions: Contributions: For research articles with multiple authors, include a brief paragraph outlining each author's contributions using the following format: “Conceptualization, Fidel Huisa Mamani; methodology, Americo Arizaca Avalos and Wilber Pastor Contreras; software, Maikol Huisa Valvivia; validation, Mishell Julisa Mamani Flores and Fidel Huisa Mamani; formal analysis, Americo Arizaca Avalos; investigation, Wilber Pastor Contreras; resources, Fidel Huisa Mamani; data curation, Wilber Pastor Contreras and Maikol Huisa Valdivia ; writ-ing—original draft preparation, Americo Arizaca Avalos and Fidel Huisa Mamani; supervision, Fidel Huisa Mamani; pro-ject administration, Mishell Julisa Mamani Flores; funding acquisition, Fidel Huisa Mamani. All authors have read and agreed to the published version of the manuscript.” Authorship should be restricted to individuals who have made significant contributions to the research.

Conflicts of Interest: The authors declare no conflicts of interest. The funder, the National University of the Altiplano, through its Vice-Rectorate for Research, had no role in the design of the study; in the collection, analysis, or interpretation of data; in the writing of the manuscript; or in the decision to publish the results.